Am J Nucl Med Mol Imaging 2013;3(5):384-392
www.ajnmmi.us /ISSN:2160-8407/ajnmmi1306001

Original Article

^{18}F-FDG imaging of human atherosclerotic carotid plaques reflects gene expression of the key hypoxia marker HIF-1α

Sune Folke Pedersen[1], Martin Græbe[2], Anne Mette F Hag[1], Liselotte Højgaard[1], Henrik Sillesen[2], Andreas Kjær[1]

[1]*Department of Clinical Physiology, Nuclear Medicine & PET and Cluster for Molecular Imaging, Rigshospitalet, University of Copenhagen, Blegdamsvej 9, 2100 Copenhagen, Denmark;* [2]*Department of Vascular Surgery, Rigshospitalet, University of Copenhagen, Blegdamsvej 9, 2100 Copenhagen, Denmark*

Received May 26, 2013; Accepted June 20, 2013; Epub September 19, 2013; Published September 30, 2013

Abstract: To investigate the association between gene expression of key molecular markers of hypoxia and inflammation in atherosclerotic carotid lesions with 2-deoxy-2-[^{18}F]fluoro-D-glucose (^{18}F-FDG) uptake as determined clinically by positron emission tomography (PET). Studies using PET have demonstrated ^{18}F-FDG-uptake in patients with confirmed plaques of the carotid artery. Inflammatory active or "vulnerable" plaques progressively increase in bulk, develop necrotic cores, poor vessel-wall vascularization and become prone to hypoxia. We used quantitative polymerase-chain reaction (qPCR) to determine gene expression of hypoxia-inducible factor 1α (HIF-1α) and cluster of differentiation 68 (CD68) on plaques recovered by carotid endarterectomy (CEA) in 18 patients. Gene expression was compared with ^{18}F-FDG-uptake quantified as the maximum standardized uptake value (SUV_{max}) on co-registered PET/computed tomography (CT) scans performed the day before CEA. Immunohistochemistry was used to validate target-gene protein expression. In univariate linear regression analysis HIF-1α was significantly correlated with ^{18}F-FDG-uptake (SUV_{max}) as was CD68. A two-tailed Pearson regression model demonstrated that HIF-1α and CD68 gene expression co-variated and accordingly when entering the variables into multivariate linear regression models with SUV-values as dependent variables, HIF-1α was eliminated in the final models. ^{18}F-FDG-uptake (SUV_{max}) is correlated with HIF-1α gene expression indicating an association between hypoxia and glucose metabolism *in vivo.* The marker of inflammation CD68 is also associated with ^{18}F-FDG-uptake (SUV_{max}). As CD68 and HIF-1α gene expression co-variate their information is overlapping.

Keywords: Hypoxia, ^{18}F-FDG PET/CT imaging, carotid atherosclerosis, gene expression, HIF-1α

Introduction

Today the "gold standard" for treating severe symptomatic carotid stenosis (≥ 50% stenosis) is carotid endarterectomy (CEA) combined with optimal medical therapy [1-3]. With the exception of Doppler ultrasonography the selection of patients for CEA has not improved significantly since the procedure was implemented in the 1950s [4]. Although some qualitative evaluation of the carotid plaque is possible using modern ultrasound systems, selection criteria remains largely based on the degree of carotid stenosis with connection to ipsilateral permanent or transient symptoms of thrombosis [1]. What is desired is an effective tool to identify the vulnerable plaque, so CEA would only be performed on vulnerable patients reducing the numbers needed to treat which currently is, at the best, about six to one [5].

Molecular imaging using positron emission tomography (PET) and computed tomography (CT) offers non-invasive *in vivo* molecular characterization with imaging agents such as 2-[^{18}F] fluoro-2-deoxy-D-glucose (^{18}F-FDG) which is a glucose analogue with ^{18}F substituted for the hydroxyl group at the 2' position in the glucose molecule. With a primary role in cancer imaging it has only recently been put to use in the first studies developed specifically for vascular imaging [6].

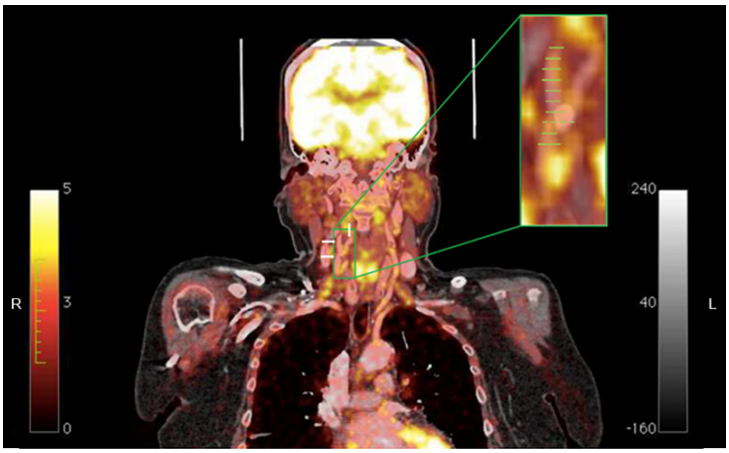

Figure 1. Coronal contrast enhanced CT-image of the right carotid with enlarged PET/CT insert. *Carotis communis and carotis internae dxt:* white arrows pointing right, *carotis externae dxt:* single white arrow pointing down. Inserted and enlarged is the fused ^{18}FDG-PET/CT modality; yellow to white coloration depicts glucose-uptake intensity. Green lines indicate where the excised plaque is physically split upon recovery. The distance between two green lines is 3 mm and the total number of lines corresponds to the total size of the excised plaque from this particular patient. The dotted line indicates the level of the bifurcation. ROIs are drawn on transaxial images, corresponding to each line on the coronal image presented here. This creates a segmented cylinder of voxels encompassing lumen, plaque and vessel wall from where the SUV values are noted. Importantly the size of the excised plaque determines the number of slices and thus corresponding ROIs on the PET/CT data. Note the calcified plaque in the bifurcation ranging from the distal common carotid artery, past the bulb and protruding into the internal carotid artery. CT = computed tomography; ^{18}FDG-PET = ^{18}F-flurodeoxyglucose-positron emission tomography; ROI = region of interest; SUV = standardized uptake value.

In humans, the vulnerable atherosclerotic lesion is characterized by intraplaque molecular and cellular processes tied to hypoxia and inflammation. Recent *in vivo* evidence of hypoxia co-localizing with foam-cells and macrophage-rich areas of atherosclerotic plaques have been reported in rabbits [7] as well as in humans [8]. The cellular response to tissue hypoxia is mobilization and assembly of a heterodimeric transcription factor consisting of hypoxia-inducible factor (HIF) subtype 1α and HIF-1β which mediate transcription initiation through binding of promoter sequences: hypoxia response elements (HREs). Whereas HIF-1β is constitutively expressed, transcriptional regulation of the HIFα subunit encoding mRNA has been recorded in hypoxic human macrophages [9] and lung epithelial cells [10].

Monocytes are multifaceted cells that may differentiate to inflammatory active cells; macrophages which may again transform and become foam cells. Macrophages play a paramount role in atherogenesis of the advanced human atherosclerotic plaques [11]. Macrophages are characterized by the type D scavenger receptor CD68 which may therefore be used as a macrophage and inflammation marker [12].

It has been demonstrated, *in vitro,* that hypoxia stimulated macrophages increase their rate of [^{3}H]-2-deoxyglucose (^{3}H-2dG) uptake *per se* [13]. ^{18}F-FDG is a glucose analogue which enables *in vivo* visualization of tissues with an elevated level of glycolysis by a process of metabolic trapping [14]. ^{3}H-2dG is a radiotracer analogue to ^{18}F-FDG and therefore ^{18}F-FDG may potentially reflect hypoxia [15, 16].

The aim of the present study was therefore to determine whether ^{18}F-FDG can be used *in vivo* as a surrogate marker of tissue hypoxia and plaque inflammation in atherosclerotic carotid disease. To do so, we determined mRNA levels of HIF-1α and CD68 in removed plaques by quantitative polymerase chain-reaction (qPCR) and compared these results with ^{18}F-FDG uptake performed just prior to surgery in patients undergoing CEA for symptomatic carotid stenosis. Additionally, qualitative protein expression of selected markers was validated by immunohistochemical detection.

Materials and methods

Ethics statement

This study was approved by the Danish National Committee on Biomedical Research Ethics (Jr. no: 0120065513) and all participants gave written informed consent on inclusion.

Patients

Patients (n = 18, five female and 13 male patients, aged 55-85 years, median 70 years)

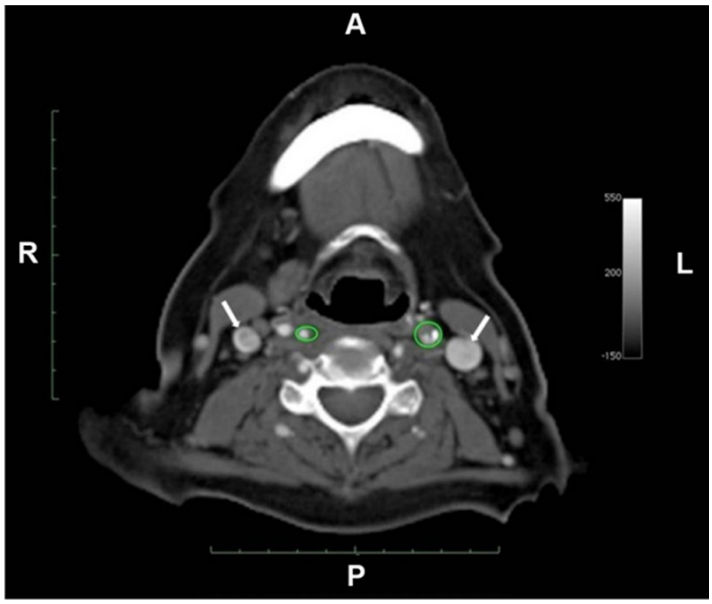

Figure 2. Contrast enhanced CT; diagnostic CTA performed with intravenous injection of contrast with bolus tracking of the ascending aorta and a cutoff value of 80 HU. In green are ROIs encircling the left and right internal carotid artery, white arrows point to the jugular veins. CT = computed tomography, CTA = CT angiography, HU = Hounsfield units, ROI = region of interest.

with clinical symptoms of cerebral vascular events, such as transient ischemic attack (TIA) and ipsilateral transient visual obscuration (*amaurosis fugax*) during the last three months and scheduled for CEA were included in the study. Internal carotid artery stenosis ipsilateral to the symptomatic hemisphere was confirmed by ultrasound and patients were then scheduled to undergo ^{18}F-FDG-PET/CT imaging prior to CEA.

^{18}F-FDG-positron emission tomography

Automatic co-registration of data was achieved using a true hybrid PET/CT scanner; the Biograph 16 (Siemens AG Healthcare Sector, Erlangen, Germany). Overnight fasting patients were administered an intravenous bolus of 400 MBq ^{18}F-FDG (364-434 MBq) and emission from a single frame over the neck was acquired in four minutes at three hours after ^{18}F-FDG administration. We have previously found 3 h post-injection and SUV_{max} to be the most robust option for overcoming the issue of high luminal blood pool ^{18}F-FDG activity, as well as being comparable to the TBR (target to background ratio) used by other investigators. Therefore we consider the 3 h SUV_{max} protocol optimal for carotid vascular imaging [17, 18]. A four minute scan was elected over the standard three minutes of a clinical scan to compensate for radiotracer decay. Before each PET acquisition a low dose (120 keV, 50 mA) CT was carried out for attenuation correction and after the second PET acquisition a final diagnostic high dose (120 keV, 200 mA) CT-angiography (CTA) was made with intravenous injection of 100 ml Optiray™ 300 mg/mL (Mallinckrodt Inc. St. Louis, MO USA) using bolus tracking in the ascending aorta with a cutoff value of 80 Hounsfield units.

Image reconstruction and analysis

Image reconstruction was performed using a standard algorithm (OSEM2D) on a dedicated Siemens workstation (SynGo Somaris/5 for WinNT 5.1, Siemens AG, Berlin) with Gaussian filtering of 3 mm, 4 iterations and 8 subsets. Matrix size was set to 256 x 256 x 55 voxels, with a voxel size of 1 x 1 mm. The transverse slice thickness was set to 3 mm and the advanced open source PACS station DICOM viewer OsiriX v. 2.7.5 (http://www.osirix-viewer.com) was used to place regions of interest (ROIs). Guided by CTA, ROIs were constructed on transaxial datasets around the common carotid artery and the internal carotid artery starting at the flow divider (bifurcature) and then every 3 mm proximally and distally covering the entire plaque ensuring the inclusion of arterial wall, plaque and lumen. The ROIs were then connected by the software creating a segmented digital cylinder of voxels or digital “slices” corresponding to the physical slices of the excised plaque. From these voxels the co-registered PET data enabled calculation of the maximal standardized uptake value (SUV_{max}) which was noted. Alignment of excised plaques to corresponding transverse image sections (voxels) was ensured by measurements of bi-directional distance of plaque from the bifurcation as noted pre-operatively.

Tissue samples

The day after PET imaging, the patients underwent carotid endarterectomy and the lesion tis-

Table 1. Primers and probes

Gene	Forward primer (5'-3')*	Reverse primer (5'-3')*	5' fluorophore†	Probe (5'-3')*	3' quencher‡	Amplicon length (bp)
HIF1α	agcagtctatttatattttc-taca	agagcattaatgtaaat-taagtag	FAM	tagaagcctggcta-caatactgca	BHQ1	125
CD68	caatggttcccagccct-gtg	tccctggaccttggtttt-gttg	FAM	ccacctccaagccca-gattcagattcgag	BHQ1	134
TBP	ggttgtaaacttgaccta-aag	gttcgtggctctcttatc	FAM	tgattaccgcagcaaaccgc	BHQ1	134
RPLP	gacggattacaccttccc	gactcttccttggcttca	Cy5	ccttcttggctgatccatctgc	BHQ2	139

*Nucleic acid sequence of primers and probes. †Fluorophores used: Cy5; Cyanine fluorophore, FAM; Fluorescein amidite. ‡Quenchers are non-fluorescent chromophores quenching non-hydrolysed probes by fluorescence resonance energy transfer (FRET): BHQ1; black hole quencher 1 deoxythymidine, BHQ2; black hole quencher 2 deoxythymidine.

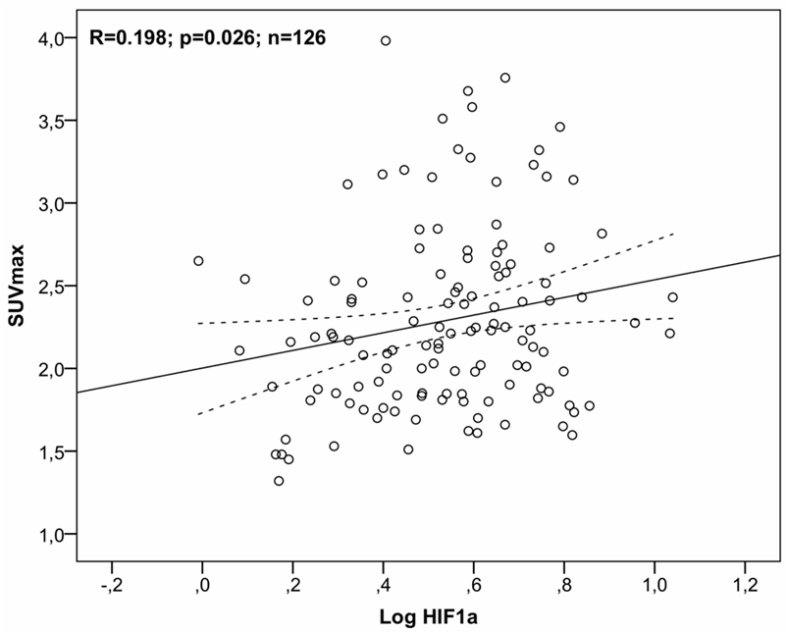

Figure 3. Gene expression; correlation to SUV_{max}. Univariate linear regression analysis of gene expression of HIF-1α relative to SUV_{max} as an expression of ^{18}F-FDG-uptake for all patients and all lesion slices (n = 126). Note log-transformation of gene expression data. The 95% confidence interval is indicated by the broken line. ^{18}F-FDG = 2-[^{18}F] fluoro-2-deoxy-D-glucose; HIF-1α = hypoxia inducible factor 1α; SUV_{max} = maximum standardized uptake value.

sue was removed *in toto* along with a macroscopically normal section of the superior thyroid artery which was used as reference tissue. The excised lesion was cut into ~3 mm slices corresponding to the transverse image sections (**Figures 1** and **2**) and stored for 24 hours at 4°C in RNAlater® (Ambion (Europe) Limited, Cambridgeshire, UK). The reference tissue was conserved *in toto*, but otherwise treated in an identical manner. The following day the RNAlater® was drained away and the samples stored at -80°C until RNA extraction (n = 126 lesion slices).

RNA extraction and cDNA synthesis

Total RNA was isolated using TRI Reagent® in accordance with the protocol of the manufacturer (Molecular Research Center Inc., Cincinnati, USA). Total RNA (10 ng) was reverse transcribed using the AffinityScript™ QPCR cDNA Synthesis Kit in accordance with the protocol of the manufacturer (Stratagene, La Jolla, CA, USA, cat. #600559).

Identifying the optimal reference gene

Using a methodology previously described [19, 20], we found when testing reference tissue against atherosclerotic tissue, that a combination of TATAA-box binding protein (TBP) and 60S acidic ribosomal protein P0 (RPLP) were optimal reference genes.

Quantitative real-time PCR (qPCR)

Gene expression was quantified on Mx3000P® or Mx3005P™ real-time PCR systems (Stratagene, La Jolla, CA, USA). Beacon Designer™ 7.90 (PREMIER Biosoft, Palo Alto, CA, USA) was utilized for primer and dual-

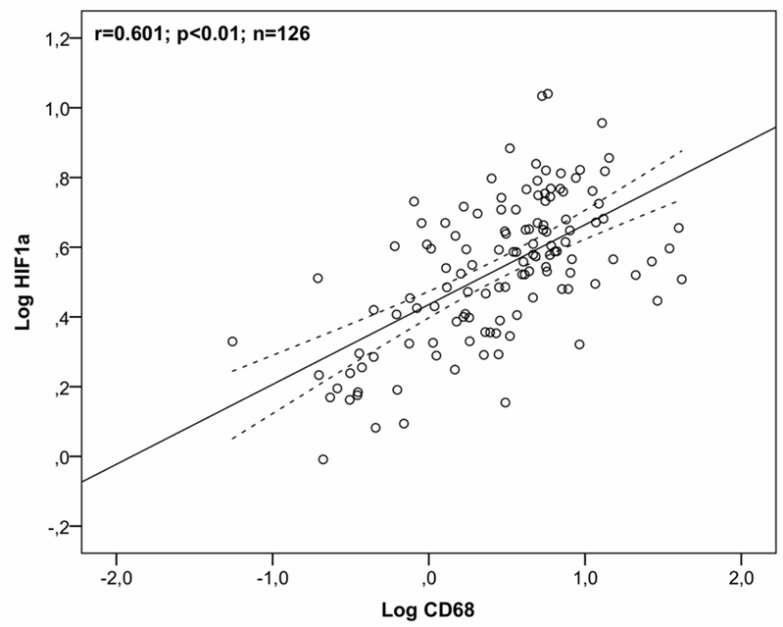

Figure 4. Correlation between CD68 and HIF-1α. Scatterplot of a two-tailed Pearson correlation analysis of gene expression of CD68 and HIF-1α for all patients and all lesion slices (n = 126). Note log-transformation of gene expression data. The 95% confidence interval is indicated by the broken line. CD68 = cluster of differentiation 68; HIF1α = hypoxia inducible factor 1α.

labeled hydrolysis (TaqMan®) probe design and the sequences of the genes of interest (GOIs) were analyzed for sequence homology concomitantly using the Basic Local Alignment Search Tool (BLAST). Two GOIs; CD68 (Gene ID: NM_0001251) and HIF-1α (Gene ID: NM_001530.3) as well as the reference genes TBP (Gene ID: NM_003194.4) and RPLP (Gene ID: NM_001002.3) were analyzed. For details of primers and probes, please refer to **Table 1**.

QPCR data-analysis

Quantitative real-time PCR data were analyzed using the qbase^{PLUS} software package (Biogazelle NV, Zwijnaarde, Belgium). In short: Normalized relative quantities (NRQs) were calculated by a generalized qbase^{PLUS} model consisting of a modified delta-delta-Cq ($2^{\Delta\Delta Cq}$) procedure including the application of multiple reference gene normalization [21, 22].

Immunohistochemistry

Using a streptavidin-peroxidase system (Vector Labs, Burlingame, CA 94010, USA) with 3,3'-Diaminobenzidine (DAB) as the chromogenic compound (Kem-en-tec, Taastrup, Denmark) slides were incubated with primary antibody diluted in 2% BSA overnight at 5°C in a moisture chamber; HIF-1α rabbit anti-human (1:100, Acris Antibodies GmbH, Herford, Germany) and CD68 mouse-anti human (1:3,000, clone KP1, Dako, Glostrup, Denmark). For HIF-1α negative controls were performed as species-matched normal serum initially diluted with PBS to a total protein concentration identical to that of the primary antibody and then to the working solution of the primary antibodies using 2% BSA. For CD68 a ready-to use FLEX control (Dako, Glostrup, Denmark) was used. Counterstaining was performed in Mayer's acidic hematoxylin.

Statistical analysis

All statistical analyses were performed using the SPSS 20 statistical software (IBM Corporation. Armonk, New York, USA). Univariate linear regression was performed between the molecular markers HIF-1α and CD68 and SUV_{max} of ^{18}F-FDG-uptake. We tested whether patients themselves were significant as co-variates by entering them in an initial multivariate analysis. This was not the case and thus ^{18}F-FDG-uptake was not patient dependent and further analyses were performed on a slice basis. Subsequent multivariate analysis was performed with backward elimination. Fold change in gene expression measurements were log-transformed to ensure Gaussian distribution as confirmed by one-sample Kolmogorov-Smirnov test. A scatterplot and two-tailed Pearson correlation analysis was performed to explore the relationship between CD68 and HIF-1α gene expression profiles. All statistical results were considered significant when $p < 0.05$.

Results

Gene expression: relation to SUV_{max}

Based on previous studies SUV_{max} was chosen as the best correlate of ^{18}F-FDG uptake with gene expression. We found significant correlations with ^{18}F-FDG-uptake calculated as SUV_{max}

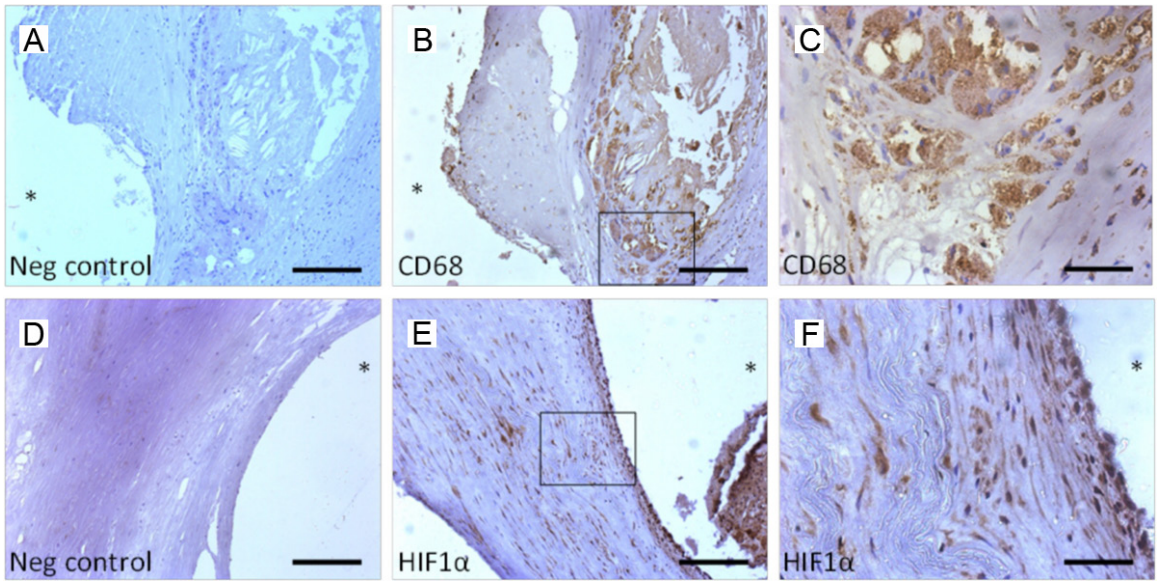

Figure 5. Immunohistochemical stainings. Immunohistochemical stains of CD68 and HIF1α: Negative control stains (left panel x 100 magnification, panel A and D). Immunohistochemical stain as indicated in each sub-panel lower left corner (middle panel x 100 magnification, panel B and E). Insert boxes indicate magnified areas that are shown in (right panel x 400 magnification, panel C and F). Scale bars: 200 μm two left columns and 50 μm right columns. (*) arterial lumen. CD68 = cluster of differentiation 68; HIF-1α = hypoxia inducible factor 1α.

with gene expression of both HIF-1α (r = 0.198, p = 0.026; **Figure 3**) and CD68 (r = 0.397, p < 0.0001). To determine the independent predictive value of HIF-1α and CD68 gene expression for ^{18}F-FDG uptake, measured as SUV_{max}, the variables were then entered into a multivariate linear regression model. It was found that HIF-1α was eliminated, leaving CD68 (β = 0.407, SE = 0.085, standardized β = 0.397, p < 0.0001) in the final model (r^2 = 0.157, p < 0.0001) which means that 16% of ^{18}F-FDG uptake can be explained by CD68 gene expression alone.

Gene expression: interrelation of CD68 and HIF-1α

As macrophage presence has been found to co-localize with hypoxic areas of atherosclerotic plaques, correlation analysis was used to investigate the relation between CD68 and HIF-1α gene expression. A significant relationship between gene expression of CD68 and HIF-1α was found in a two-tailed Pearson correlation analysis (r = 0.601, p < 0.01) indicating that CD68 and HIF-1α gene expression co-variate; **Figure 4**.

Immunohistochemistry

To confirm protein expression of gene expression targets qualitative immunohistochemical staining for the molecular markers HIF-1α and CD68 was performed. The results can be seen in **Figure 5**.

Discussion

This study is the first to demonstrate that ^{18}F-FDG-uptake (SUV_{max}) in atherosclerotic lesions in patients is associated with the key molecular marker of hypoxia HIF-1α. This result is in line with the hypothesis we previously suggested as an explanation to our earlier findings: That micro vessel density, but not neoangiogenesis is associated with ^{18}F-FDG-uptake, likely through a connection between hypoxia and inflammation [20]. To be concise that study found that micro vessel density was significantly, but inversely correlated with ^{18}F-FDG uptake. This is in line with earlier findings in pigs which indicated that low micro vessel density and resulting hypoxic conditions could lead to microinflammation and atherogenesis, however that was a non-imaging study [23]. Molecular imaging of angiogenesis with PET is likely to be based on the tripeptide Arg-Gly-Asp (RGD) which is a motif on vitronectin, a glycoprotein abundant in the extracellular matrix. Angiogenic sprouting is initiated by endothelial cells (ECs) which express the integrin dimer $\alpha_V\beta_3$; a receptor for the RGD motif. Interaction between RGD

and $\alpha_V\beta_3$ enable migration of sprouting ECs and therefore also provide an imaging target for angiogenesis. Initial studies in atherosclerotic mice used ^{18}F-galacto-RGD as an angiogenesis tracer [24]. Unfortunately ^{18}F-galacto-RGD is highly difficult to produce and its use is therefore diminishing, however promising new alternatives based on RGD are now emerging [25].

The connection of hypoxia and inflammation is based on a complex interrelationship between the HIF-1α transcription factor and the transcription factor nuclear factor-κB (NF-κB) which is a central regulator of innate immunity. In short, blood marrow derived monocytes were demonstrated to depend on the NF-κB subunit IKKβ for HIF-1α gene expression. Without IKKβ HIF-1α mRNA was down regulated in macrophages challenged with hypoxia *in vitro* as well as in an *in vivo* mouse model of hypoxia [26]. Adding to the complexity IKKβ catalytic activity (and HIF-1α subunit stabilization) is repressed by hydroxylation by O_2 dependent prolyl hydroxylases (PHDs) whose own activity is diminished by hypoxia *per se*.

When HIF-1α subunit stabilization occurs in a low oxygen environment, HIF-1 can translocate to the cell nucleus and directly bind to gene promoters of pattern recognition receptors; the toll like receptors (TLR) TLR-2 and TLR-6. *In vitro* evidence using human cells confirmed that TLR2 and TLR6 mRNA and protein is upregulated by HIF-1 in hypoxia [27]. The connection between HIF-1 and TLRs may explain part of the link between hypoxia and inflammation. Hypoxia thus induces NF-κB, HIF-1α activity and TLR expression driving a combined response linking hypoxia and inflammation on the molecular level [28].

Furthermore it was confirmed that CD68 gene expression lends independent information to ^{18}F-FDG-uptake (SUV_{max}). The correlation of CD68 gene expression with ^{18}F-FDG-uptake has previously been described [20]. In addition we used immunohistochemistry in this study to confirm that CD68, as well as HIF-1α protein, were expressed in atherosclerotic carotid plaques. However using correlation analysis we found that CD68 and HIF-1α gene expression co-variates (**Figure 3**). In itself this is not surprising; as described the intertwined molecular and cellular mechanisms between inflammation and hypoxia means we cannot, to some extent, have one without the other [29, 30]. Therefore HIF-1α was eliminated in the multivariate analysis only due to its lesser strength as a predictor of ^{18}F-FDG-uptake as compared to CD68.

Clinically the impact of molecular characterization of atherosclerotic plaques using PET would be improved selection criteria for CEA opening the possibility for a higher degree of individualized patient treatment. Imaging atherosclerosis is still a new discipline and ^{18}F-FDG is a natural first choice as tracer, however other tracers specific to targets known to be expressed in plaques are being introduced [31, 32]. The ultimate goal is to identify a biomarker that is only expressed in vulnerable atherosclerotic plaques and to subsequently develop a tracer which would enable identification of patients eligible for CEA thus reducing the need to treat ratio in a one-stop-shop solution.

Conclusions

We found that ^{18}F-FDG-uptake (SUV_{max}) correlated well with gene expression of the key marker of hypoxia HIF-1α. In addition ^{18}F-FDG-uptake was correlated with the marker of inflammation CD68. Gene expression of the molecular markers CD68 and HIF-1α co-variate and are therefore both associated with ^{18}F-FDG-uptake. Qualitative immunohistochemical analyses validated expression of the selected genetic markers on the protein level.

Acknowledgements

The financial support from The Danish Heart Foundation, The Research Fund of Rigshospitalet, The Danish Medical Research Council, The John and Birthe Meyer Foundation, General-consul Friedrich Bøhm and daughter Else Bøhms Foundation, Tove and Richard Severin Hansens Grant, The Oticon Foundation and finally The Refuge of Løgumkloster is gratefully acknowledged. The PET/CT scanner was donated by the John and Birthe Meyer Foundation. The authors wish to thank all medical laboratory technologists involved in PET/CT acquisition.

Disclosure of conflict of interest

The authors declare no conflict of interests.

Address correspondence to: Sune Folke Pedersen, MSc, Cluster for Molecular Imaging, Department of Biomedical Sciences, Faculty of Health, Room 12.3.38, University of Copenhagen, Blegdamsvej 3B, 2200 Copenhagen N, Denmark. Tel: +45 35326007; Fax: +45 35327546; E-mail: sfolkep@sund.ku.dk; Dr. Andreas Kjær, Department of Clinical Physiology, Nuclear Medicine & PET and Cluster for Molecular Imaging, Rigshospitalet, University of Copenhagen, Blegdamsvej 9, 2100 Copenhagen, Denmark. E-mail: akjaer@sund.ku.dk

References

[1] Hobson RW, Mackey WC, Ascher E, Murad MH, Calligaro KD, Comerota AJ, Montori VM, Eskandari MK, Massop DW, Bush RL, Lal BK and Perler BA. Management of atherosclerotic carotid artery disease: clinical practice guidelines of the Society for Vascular Surgery. J Vasc Surg 2008; 48: 480-486.

[2] Rerkasem K and Rothwell PM. Carotid endarterectomy for symptomatic carotid stenosis. Cochrane Database Syst Rev 2011; CD001081.

[3] Brott TG, Hobson RW, Howard G, Roubin GS, Clark WM, Brooks W, Mackey A, Hill MD, Leimgruber PP, Sheffet AJ, Howard VJ, Moore WS, Voeks JH, Hopkins LN, Cutlip DE, Cohen DJ, Popma JJ, Ferguson RD, Cohen SN, Blackshear JL, Silver FL, Mohr JP, Lal BK and Meschia JF. Stenting versus endarterectomy for treatment of carotid-artery stenosis. N Engl J Med 2010; 363: 11-23.

[4] Keitzer WF, Lichti EL and DeWeese MS. Clinical evaluation and correction of carotid artery occlusive disease. Use of the Doppler ultrasonic flowmeter. Am J Surg 1972; 124: 697-700.

[5] Chaturvedi S, Bruno A, Feasby T, Holloway R, Benavente O, Cohen SN, Cote R, Hess D, Saver J, Spence JD, Stern B and Wilterdink J. Carotid endarterectomy--an evidence-based review: report of the Therapeutics and Technology Assessment Subcommittee of the American Academy of Neurology. Neurology 2005; 65: 794-801.

[6] Rudd JH, Warburton EA, Fryer TD, Jones HA, Clark JC, Antoun N, Johnstrom P, Davenport AP, Kirkpatrick PJ, Arch BN, Pickard JD and Weissberg PL. Imaging atherosclerotic plaque inflammation with [18F]-fluorodeoxyglucose positron emission tomography. Circulation 2002; 105: 2708-2711.

[7] Bjornheden T, Levin M, Evaldsson M and Wiklund O. Evidence of hypoxic areas within the arterial wall in vivo. Arterioscler Thromb Vasc Biol 1999; 19: 870-876.

[8] Sluimer JC, Gasc JM, van Wanroij JL, Kisters N, Groeneweg M, Sollewijn Gelpke MD, Cleutjens JP, van den Akker LH, Corvol P, Wouters BG, Daemen MJ and Bijnens AP. Hypoxia, hypoxia-inducible transcription factor and macrophages in human atherosclerotic plaques are correlated with intraplaque angiogenesis. J Am Coll Cardiol 2008; 51: 1258-1265.

[9] Frede S, Stockmann C, Freitag P and Fandrey J. Bacterial lipopolysaccharide induces HIF-1 activation in human monocytes via p44/42 MAPK and NF-kappaB. Biochem J 2006; 396: 517-527.

[10] Uchida T, Rossignol F, Matthay MA, Mounier R, Couette S, Clottes E and Clerici C. Prolonged hypoxia differentially regulates hypoxia-inducible factor (HIF)-1alpha and HIF-2alpha expression in lung epithelial cells: implication of natural antisense HIF-1alpha. J Biol Chem 2004; 279: 14871-14878.

[11] Shashkin P, Dragulev B and Ley K. Macrophage differentiation to foam cells. Curr Pharm Des 2005; 11: 3061-3072.

[12] Greaves DR and Gordon S. Macrophage-specific gene expression: current paradigms and future challenges. Int J Hematol 2002; 76: 6-15.

[13] Folco EJ, Sheikine Y, Rocha VZ, Christen T, Shvartz E, Sukhova GK, Di Carli MF and Libby P. Hypoxia but not inflammation augments glucose uptake in human macrophages: Implications for imaging atherosclerosis with 18fluorine-labeled 2-deoxy-D-glucose positron emission tomography. J Am Coll Cardiol 2011; 58: 603-614.

[14] Gallagher BM, Fowler JS, Gutterson NI, MacGregor RR, Wan CN and Wolf AP. Metabolic trapping as a principle of oradiopharmaceutical design: some factors resposible for the biodistribution of [18F] 2-deoxy-2-fluoro-D-glucose. J Nucl Med 1978; 19: 1154-1161.

[15] Doenst T and Taegtmeyer H. Kinetic differences and similarities among 3 tracers of myocardial glucose uptake. J Nucl Med 2000; 41: 488-492.

[16] Shozushima M, Tsutsumi R, Terasaki K, Sato S, Nakamura R and Sakamaki K. Augmentation effects of lymphocyte activation by antigen-presenting macrophages on FDG uptake. Ann Nucl Med 2003; 17: 555-560.

[17] Graebe M, Borgwardt L, Hojgaard L, Sillesen H and Kjaer A. When to image carotid plaque inflammation with FDG PET/CT. Nucl Med Commun 2010; 31: 773-779.

[18] Graebe M, Pedersen SF, Borgwardt L, Hojgaard L, Sillesen H and Kjaer A. Molecular pathology in vulnerable carotid plaques: correlation with [18]-fluorodeoxyglucose positron emission tomography (FDG-PET). Eur J Vasc Endovasc Surg 2009; 37: 714-721.

[19] Vandesompele J, De PK, Pattyn F, Poppe B, Van RN, De PA and Speleman F. Accurate nor-

malization of real-time quantitative RT-PCR data by geometric averaging of multiple internal control genes. Genome Biol 2002; 3: RESEARCH0034.

[20] Pedersen SF, Graebe M, Hag AM, Hoejgaard L, Sillesen H and Kjaer A. Microvessel Density But Not Neoangiogenesis Is Associated with (18)F-FDG Uptake in Human Atherosclerotic Carotid Plaques. Mol Imaging Biol 2012; 14: 384-92.

[21] Hellemans J, Mortier G, De PA, Speleman F and Vandesompele J. qBase relative quantification framework and software for management and automated analysis of real-time quantitative PCR data. Genome Biol 2007; 8: R19.

[22] Livak KJ and Schmittgen TD. Analysis of relative gene expression data using real-time quantitative PCR and the 2(-Delta Delta C(T)) Method. Methods 2001; 25: 402-408.

[23] Gossl M, Versari D, Lerman LO, Chade AR, Beighley PE, Erbel R and Ritman EL. Low vasa vasorum densities correlate with inflammation and subintimal thickening: potential role in location--determination of atherogenesis. Atherosclerosis 2009; 206: 362-368.

[24] Laitinen I, Saraste A, Weidl E, Poethko T, Weber AW, Nekolla SG, Leppanen P, Yla-Herttuala S, Holzlwimmer G, Walch A, Esposito I, Wester HJ, Knuuti J and Schwaiger M. Evaluation of alphavbeta3 integrin-targeted positron emission tomography tracer 18F-galacto-RGD for imaging of vascular inflammation in atherosclerotic mice. Circ Cardiovasc Imaging 2009; 2: 331-338.

[25] Oxboel J, Schjoeth-Eskesen C, El-Ali HH, Madsen J and Kjaer A. (64)Cu-NODAGA-c(RGDyK) Is a Promising New Angiogenesis PET Tracer: Correlation between Tumor Uptake and Integrin alpha(V)beta(3) Expression in Human Neuroendocrine Tumor Xenografts. Int J Mol Imaging 2012; 2012: 379807.

[26] Rius J, Guma M, Schachtrup C, Akassoglou K, Zinkernagel AS, Nizet V, Johnson RS, Haddad GG and Karin M. NF-kappaB links innate immunity to the hypoxic response through transcriptional regulation of HIF-1alpha. Nature 2008; 453: 807-811.

[27] Kuhlicke J, Frick JS, Morote-Garcia JC, Rosenberger P and Eltzschig HK. Hypoxia inducible factor (HIF)-1 coordinates induction of Toll-like receptors TLR2 and TLR6 during hypoxia. PLoS One 2007; 2: e1364.

[28] Cummins EP, Berra E, Comerford KM, Ginouves A, Fitzgerald KT, Seeballuck F, Godson C, Nielsen JE, Moynagh P, Pouyssegur J and Taylor CT. Prolyl hydroxylase-1 negatively regulates IkappaB kinase-beta, giving insight into hypoxia-induced NFkappaB activity. Proc Natl Acad Sci U S A 2006; 103: 18154-18159.

[29] Eltzschig HK and Carmeliet P. Hypoxia and inflammation. N Engl J Med 2011; 364: 656-665.

[30] Taylor CT. Interdependent roles for hypoxia inducible factor and nuclear factor-kappaB in hypoxic inflammation. J Physiol 2008; 586: 4055-4059.

[31] Dweck MR, Chow MW, Joshi NV, Williams MC, Jones C, Fletcher AM, Richardson H, White A, McKillop G, van Beek EJ, Boon NA, Rudd JH and Newby DE. Coronary arterial 18F-sodium fluoride uptake: a novel marker of plaque biology. J Am Coll Cardiol 2012; 59: 1539-1548.

[32] Rominger A, Saam T, Vogl E, Ubleis C, la FC, Forster S, Haug A, Cumming P, Reiser MF, Nikolaou K, Bartenstein P and Hacker M. In vivo imaging of macrophage activity in the coronary arteries using 68Ga-DOTATATE PET/CT: correlation with coronary calcium burden and risk factors. J Nucl Med 2010; 51: 193-197.